Numerical solution of EMHD GO-MoS_2/H_2O flow and heat transportation toward stretching/ shrinking riga plate with joule heating and convective boundary condition

Nur Aisyah Aminuddin[1,3 a)], Nooraini Zainuddin[2, b)] , Nor Ain Azeany Mohd Nasir [3, c)] , Alinda Samsuri [4,d)] and Anuar Ishak [5, e)]

[1] *Department of Defense Science, Faculty of Defense Science and Technology, National Defence University of Malaysia, Sungai Besi Camp, 57000 Kuala Lumpur, Malaysia.*
[2] *Department of Fundamental and Applied Sciences, Faculty of Science and Information Technology, Universiti Teknologi PETRONAS, 32610 Seri Iskandar, Perak, Malaysia*
[3] *Department of Mathematics, Centre for Defence Foundation Studies, Universiti Pertahanan Nasional Malaysia, Kem Sungai Besi 57000 Kuala Lumpur, Malaysia.*
[4] *Department of Chemistry and Biology, Centre for Defence Foundation Studies, Universiti Pertahanan Nasional Malaysia, Kem Sungai Besi 57000 Kuala Lumpur, Malaysia.*
[5] *Department of Mathematical Sciences, Faculty of Science and Technology, Universiti Kebangsaan Malaysia, 43600 UKM Bangi, Selangor, Malaysia*

[a)] nuraisyahamndn@gmail.com
[b)] aini_zainuddin@utp.edu.my
[c)] Corresponding author: norainazeany@upnm.edu.my
[d)] alinda@upnm.edu.my
[e)] anuar_mi@ukm.edu.my

Abstract. This research includes a convective boundary condition and joule heating in a numerical study of the EMHD stagnation point flow of a GO-MoS_2/water hybrid nanofluid across a contracting sheet. The governing partial differential equations are transformed using a similarity criterion into non-linear ordinary differential equations of third and second order. The bvp4c solver is then used to perform the numerical solution of these equations. Graphs and discussions of the computational results for the skin friction coefficient, local Nusselt number, velocity, and temperature profiles for a range of physical parameter values are provided. Dual solutions provide intriguing behaviour for specific governing factors. According to the findings, the magnetic field parameter, Eckert number and the radiation parameter all have a role in determining the velocity and the temperature. Significant changes occur in the local Nusselt number and skin friction coefficient when suction is present. It is noted that the performance of skin friction is enhanced with the Hartmann number and suction parameter, while the radiation and Biot numbers can improve the heat transfer rate.

INTRODUCTION

In recent years, hybrid nanofluids have garnered considerable interest due to their unique properties and potential applications in a wide range of fields. Hybrid nanofluids refer to colloidal suspension types comprising conventional base fluids and nanoparticles. These nanoparticles are either derived from diverse materials or possess distinct properties. Hybrid nanofluid has a lot of application usage in various fields such as biomedical, engineering in cooling or heating and many more [1]. For instance, in the biomedical field, hybrid nanofluids have been explored in the context of drug delivery systems, wherein nanoparticles are employed to encapsulate drugs and facilitate their

targeted delivery to specific anatomical sites within the human body [2]. Contrast agents for improved magnetic resonance imaging (MRI) or computerized tomography (CT) scans are among the imaging techniques where they find application. Meanwhile, for application in the aerospace and automotive fields, hybrid nanofluids exhibit promising capabilities in augmenting the operational efficiency of heat exchangers and radiators employed in the aviation and automotive industries [3]. Enhancing the thermal conductivity and heat transfer properties can facilitate the cooling of engines and augment overall energy efficiency. Alkuhayli [4] presented research endeavours to examine the phenomenon of heat transfer in a hybrid nanofluid that is placed in motion by means of a rotating disc. The aqueous nanofluid comprises nanoparticles of copper and dioxide and is subject to a uniform magnetic field. According to their report, the Nusselt number within the local vicinity experiences an increment upon an increase in the variable thermal conductivity parameter. However, it undergoes a decrement with an increase in nanoparticle concentration, while it experiences an increase with the thermal radiation parameter.

Electromagnetohydrodynamic (EMHD) is the investigation of liquid with electrical conductivity under the influences of magnetic and electric fields. In securing the intended outcomes from a poor conductivity liquid, a supplementary external electric field would be of use to regulate the flow. One of the commonly utilized devices of EMHD is the Riga plate, which was introduced by Gailitis and Lielausus [5]. It comprises electrodes and magnets that are placed alternatively over a plate. The fluid flow can be regulated by this device as it is hydromagnetically induced and will form an electromagnetic field that generates a force called Lorentz. The force gives impact to the boundary layer flow and can balance the flow. The usage of the Riga plate is popular in various applications such as biomedical drug targeting, heat reactors, geophysics, submarines, and small-sized coolers. The stagnation flow of hybrid nano liquid was scrutinized by Kayalvizhi and Kumar [6] with radiation and heat generation/sink on a porous plate, Khashi'ie et al. [7] under the influences of mixed convection, Mukhtar and Gul [8] impacted by solar radiation, Khan et al. [9] affected by buoyancy and slips, and Yahaya et al. [10] with mixed convection and radiation effects. More studies of hybrid nanofluid on a Riga wedge were examined by Souayeh et al. [11] on gold-Ag/Blood with activation energy, Sindhu et al. [12] on Al_2O_3-Ag/H_2O and Al_2O_3- TiO_2/H_2O impacted by thermal source/sink, and Ahmed et al. [13] on Fe_3O_4-Ag/H_2O between two Riga plates.

Graphene oxide (GO) is a particle that is made up of carbon, hydrogen, and oxygen. The study of graphene oxide in nanofluid for heat transfer process is emerging among scientists and researchers. This particle gained attention due to its potential to improve the thermal characteristic of a fluid. Its thermal conductivity is listed as one of the top listed particles that are commonly used for heat transfer purposes. Some industries that have been using this particle include drug delivery, cancer treatment, and cellular imaging. Dawar et al. [14] explored the radiated stagnation flow of GO-Fe_3O_4/H_2O on a non-isothermal surface and deduced that a higher concentration of graphene oxide added into the fluid leads to high temperature. This result is the same as the study by Ahmad et al. [15] on the flow of GO-Fe_3O_4/EO, Mansouri et al. [16] on the flow of Gold-GO/H_2O specifically for computer's CPU, and magnetite flow of GO/H_2O along a thin needle by Hamid et al. [17]. Dinarvand and Rostami [18] compared the flow of GO/H_2O and Fe_3O_4/H_2O in their study. They found out that the increment of GO enhanced the skin friction and Nusselt number, and the percentages are higher compared to the elevation of Fe_3O_4. Huminic et al. [19] analyzed Si-GO/H_2O and finalized that the pumping power needed for GO/H_2O and Si-GO/H_2O is higher than Si/H_2O. A study by Bharadwaj et al. [20] on the flow of CG-GO/RO+EG also stated that higher pumping power is required when the concentration of GO is elevated.

Joule heating boosts heat transfer characteristics by reducing the current to minimize destruction in the form of electrical transmission. The electrical energy transforms into thermal energy throughout the fluid flow. The employment of Joule heating can be found in several appliances like electronic device configurations, cartridge warmers, and MHD thrusters. By taking the Joule heating effect into account, Zubair et al. [21] explored squeezing magnetohydrodynamic (MHD) Casson nanofluid with viscous dissipation on a rotating porous wedge. Rasheed et al. [22] analyzed Jeffrey nanofluid over an expanding vertical cylinder under the influence of radiation, magnetic, heat generation and viscous dissipation. Jayanthi and Niranjan [23] examined MHD nanofluid on a vertical surface impacted by activation energy, radiation, and viscous dissipation. Joyce et al. [24] evaluated Al_2O_3-Cu/H_2O over a porous forward-moving plate with slips and chemical reactions. Yan et al. [25] inspected MHD Al_2O_3-Cu/H_2O on an exponentially contracting plate affected by slips. Prabakaran et al. [26] considered Al_2O_3-CNTs/H_2O flow with mixed convection in the presence of heat source/sink, radiation and magnetic field. Considering the study of stagnation area, Narayanaswamy et al. [27] did research on MHD GO-MOS_2/H_2O over a backward moving cylinder plate with the existence of Stefan blowing, slips and radiation. In contrast, Zainal et al. [28] looked over the flow of Al_2O_3-Cu/H_2O under the influence of viscous dissipation.

The utilization of convective boundary conditions was initially introduced by Aziz [29]. Based on past scholars, convective boundary condition should be considered because it is exceptionally salient in a process with high

temperature and more suitable and practical in a lot of applications. Some industries that accommodate convective boundary conditions include heat exchangers, gas turbines, material drying, nuclear plants, transpiration cooler, energy storage, and electric cables. A study by Joyce et al. [24] stated that the Biot number is a function of thermal conductivity, so the temperature of the liquid is meant to be elevated as the thermal conduction will rise when the value of the Biot number increases. This result is supported by other investigations that included the convective boundary condition, such as a study by Ashraf et al. [30] where they scrutinized the flow of Al_2O_3-Fe_3O_4/H_2O on a curved elongating surface, Zainal et al. [31] on the analysis of Al_2O_3-Cu/H_2O over a Falkner-Skan sheet, and the flow of Al_2O_3-Cu/H_2O with suction by Anuar et al. [32] However, a study by Zainal et al. [33] proved the opposite where the inclination of Biot number managed to decline the temperature profile. This is mainly because of its relationship with the thermal resistance. This result is backed up by other works, too, such as the 3-D flow of Al_2O_3-Cu/H_2O with velocity slip by Khashi'ie et al. [34] and the radiated flow of GO-Fe_2O_4/EG by Aminuddin et al. [35].

The astonishing properties of hybrid nanofluid with graphene oxide as the main article are what inspired this paper to examine it over a shrinking sheet. The objective of this study is to investigate the flow GO-MoS_2/H_2O influenced by radiation, Joule heating, and suction scrutinized over a porous moving Riga surface. Mathematical formulation in the form of partial differential equations is formed, and they are reduced into partial differential equations for numerical analysis. Numerical computation by the bvp4c solver is adapted, and the generated results include the temperature profile, velocity profile, skin friction coefficient and local Nusselt number.

MATHEMATICAL MODELLING

A sustained, two-dimensional boundary layer hybrid nanofluid (GO-MoS_2/water) near a movable horizontal Riga plate is shown in Figure 1. The mass flux constant velocity $v(x) = v_w$, where the injection parameter is denoted as $v_w > 0$ while the suction parameter is as $v_w < 0$ and when $v_w = 0$ is presumed as permeable. The surface is assumed to contract with the velocity along the x-path. T_∞ is called as ambient temperature, and T_w is the flat plate's constant temperature. Therefore, using these presumptions, the boundary layer equations will be as follows (Nasir et al. [36] and Aminuddin et al. [35]):

$$\frac{\partial u}{\partial x} + \frac{\partial v}{\partial y} = 0$$

$$u\frac{\partial u}{\partial x} + v\frac{\partial u}{\partial y} = u_e\frac{\partial u_e}{\partial x} + \frac{\mu_{hnf}}{\rho_{hnf}}\frac{\partial^2 u}{\partial y^2} + \frac{\pi j_0 M_0}{8\rho_{hnf}}e^{-\frac{\pi}{\alpha_1}y}$$

$$u\frac{\partial T}{\partial x} + v\frac{\partial T}{\partial y} = \frac{k_{hnf}}{(\rho C_p)_{hnf}}\left(\frac{\partial^2 T}{\partial y^2}\right) + \frac{\mu_{hnf}}{(\rho C_p)_{hnf}}\left(\frac{\partial u}{\partial y}\right)^2 + \frac{\sigma B_0^2}{(\rho C_p)_{hnf}}(u - u_e)^2 - \frac{1}{(\rho C_p)_{hnf}}\left(\frac{\partial q_r}{\partial y}\right)$$

With boundary conditions of:

$$u = \alpha u_w, \quad v = v_w(x), \quad -k\frac{\partial T}{\partial y} = h_f(T_f - T) \quad at\ y = 0$$

$$u \to u_e = u_0 x, \quad T \to T_\infty \quad as\ y \to \infty$$

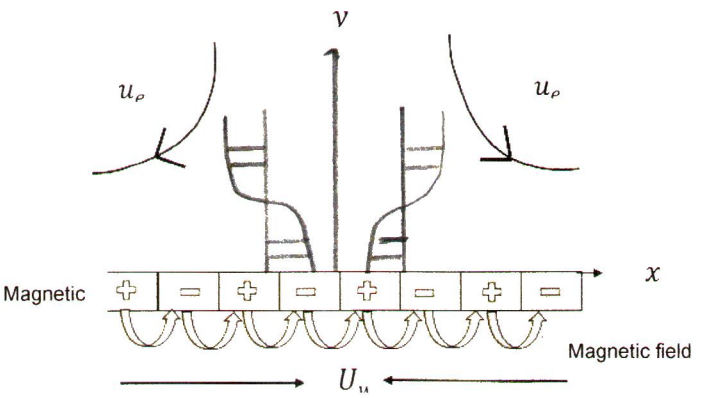

FIGURE 1. Contracting porous surface model.

Similarity variables that are suitable for transforming partial differential equations (PDEs) into ordinary differential equations (ODEs) are introduced (see Aziz et al. [37]):

$$\psi(\eta) = \sqrt{u_0 v_f}\, x f(\eta), \quad \vartheta(\eta) = \frac{T - T_\infty}{T_w - T_\infty}, \quad \eta = y\sqrt{\frac{u_0}{v_f}} \tag{5}$$

While the function of u and v are denoted as $u = \frac{\partial \psi}{\partial y}$ and $v = -\frac{\partial \psi}{\partial x}$. After some derivations, they can be defined as:

$$u = u_0 x f'(\eta), \quad v = -\sqrt{u_0 v_f} f(\eta) \tag{6}$$

Then, by substituting equations in (5) and (6) into PDEs in (1) – (4), the reduced ODEs are acquired:

$$\frac{1}{\phi_a \phi_b} f''' + f f'' - f'^2 + \frac{G}{\phi_b} e^{-\eta\Delta} + 1 = 0 \tag{7}$$

$$\left(\frac{Pr\,\phi_c}{\phi_d + Rd}\right)\vartheta'' + Ec\frac{1}{\phi_c}\left[\frac{1}{\phi_a} f''^2 + M(f' - 1)^2\right] + f\vartheta' = 0 \tag{8}$$

Subject to boundary conditions of:

$$f'(0) = \alpha, \; f(0) = s, \; -\phi_d \vartheta'(0) = Bi(1 - \vartheta) \text{ at } \eta = 0$$
$$f'(\eta) \to 1, \quad \vartheta(\eta) \to 0 \text{ as } \eta \to \infty \tag{9}$$

The parameters $G = \frac{\pi j_0 M_0}{8\rho_f u_0^2}$, $\Delta = \frac{\pi}{\alpha_1}\sqrt{\frac{v_f}{u_0}}$, $\Pr = \frac{k_f}{v_f(\rho C_p)_f}$, $Rd = \frac{16\sigma^* T_r^3}{3k^* k_f}$, $\mathrm{Ec} = \frac{U_w^2}{(T_w - T_r)(C_p)_f}$, $M = \frac{\sigma B_0^2}{u_0 \rho_f}$, $Bi = \frac{h_f}{k_f}\sqrt{\frac{v_f}{u_0}}$, s and α represent Hartmann number, dimensionless variable, Prandtl number, radiation, Eckert number, magnetic variable, Biot number, suction and expanding/contracting parameter, respectively. ϕ_a, ϕ_b, ϕ_c and ϕ_d are hybrid nanofluid parameters, where (Source: Qureshi [38]):

$$\phi_a = (1 - \phi_1)^{2.5}(1 - \phi_2)^{2.5} = \frac{\mu_f}{\mu_{hnf}}$$
$$\phi_b = (1 - \phi_2)\left[(1 - \phi_1) + \phi_1\frac{\rho_{s1}}{\rho_f}\right] + \phi_2\frac{\rho_{s2}}{\rho_f} = \frac{\rho_{hnf}}{\rho_f}$$
$$\phi_c = (1 - \phi_2)\left[(1 - \phi_1) + \phi_1\frac{(\rho C_p)_{s1}}{(\rho C_p)_f}\right] + \phi_2\frac{(\rho C_p)_{s2}}{(\rho C_p)_f} = \frac{(\rho C_p)_{hnf}}{(\rho C_p)_f}$$
$$\phi_d = \frac{k_{hnf}}{k_f} \tag{10}$$

TABLE 1. The features of thermo-physical hybrid nanofluids. (Source: Devi and Devi [39]).

Features	Hybrid Nanofluid
Density (ρ)	$\rho_{hnf} = (1-\phi_2)\left[(1-\phi_1)\rho_f + \phi_1\rho_{s1}\right] + \phi_2\rho_{s2}$
Viscosity (μ)	$\mu_{hnf} = \mu_f/(1-\phi_1)^{2.5}(1-\phi_2)^{2.5}$
Heat capacity (ρC_p)	$(\rho C_p)_{hnf} = (1-\phi_2)\left[(1-\phi_1)(\rho C_p)_f + \phi_1(\rho C_p)_{s1}\right] + \phi_2(\rho C_p)_{s2}$
Thermal conductivity (k)	$k_{hnf} = \dfrac{k_{s2} + 2k_{nf} - 2\phi_2(k_{nf} - k_{s2})}{k_{s2} + 2k_{nf} + \phi_2(k_{nf} - k_{s2})} \times k_{nf}$

TABLE 2. The values of nanoparticles and base fluid thermo-physical properties (Source: Yaseen et al. [40] and Hamid et al. [17])

Thermophysical Properties	Graphene Oxide (GO)	Molybdenum Disulphide (MoS_2)	Water (H_2O)
Thermal conductivity k	5000	34.5	0.613
Density ρ	1800	5060	997.1
Specific heat C_p	717	397.746	4179

In this paper, skin friction coefficient C_f and Nusselt number Nu_x are the physical quantities that are evaluated. They are represented by (Source: Nasir et al. [36])

$$C_f = \frac{\tau_w}{\rho_f u_w^2}, \quad Nu_x = \frac{x q_w}{k_f(T_w - T_\infty)} \tag{11}$$

$\tau_w = \mu_{hnf}\left(\frac{\partial u}{\partial y}\right)_{y=0}$ depicts the shear stress and $q_w = -k_{hnf}(1+Rd)\left(\frac{\partial T}{\partial y}\right)_{y=0}$ denotes the heat flux. The physical quantities in (11) can be derived by using the similarity transformations in (5),

$$Re_x^{\frac{1}{2}}\, C_f = \frac{1}{\phi_a} f'', \qquad Re_x^{-\frac{1}{2}} Nu_x = -\phi_d(1+Rd)\vartheta' \tag{12}$$

Where $Re_x = \frac{u_0 x^2}{\nu_f}$ is the local Reynolds number.

DISCUSSION

In this paper, the numerical computation is executed by using the bvp4c solver built-in MATLAB, as this software has the ability to work out complicated boundary conditions that come together with the PDEs. The hybrid nanofluid is made up from the combination of graphene oxide (GO), molybdenum disulphine (MoS_2) and water (H_2O) with Prandtl number of Pr = 6.2. GO and MoS_2 are represented by ϕ_1 and ϕ_2, respectively. The results for this analysis which are the skin friction, Nusselt number, temperature, and velocity profiles, are obtained by differing the value of parameter variables.

The increment of Hartmann number G surges the value of skin friction and Nusselt number, as illustrated in Figure 3 (a) and 3 (b). The support gained from the utilization of Riga plate to produces a powerful Lorentz force that somehow drags the particles over the surface, thus influencing the frictional force generated. As G grows, higher rate of heat is transferred out of the fluid, which explains the escalation of Nusselt number. Moreover, the separation of boundary layer also decelerates as the critical point keeps getting smaller, such that that $\alpha_c = -2.9302$ (G =0.01), $\alpha_c = -2.9775$ (G =0.08) and $\alpha_c = -2.9908$ (G =0.1).

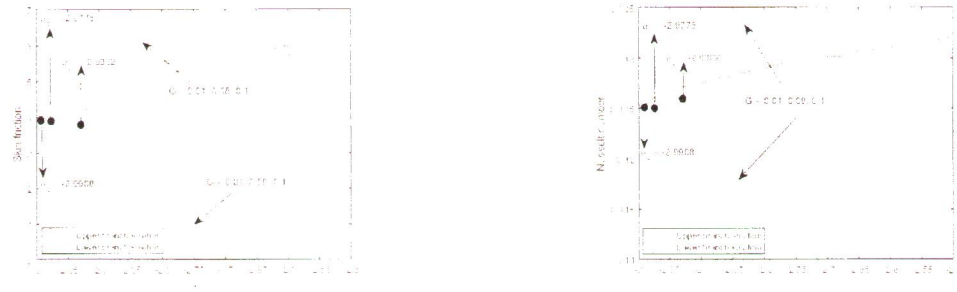

(a) (b)

FIGURE 3. (a) $C_f Re_x^{\frac{1}{2}}$ for varied G, (b) $Nu_x Re_x^{-\frac{1}{2}}$ for varied G *and* Δ= 0.1, Rd = 0.5, Ec = 0.01, M = 0.1, s= 2, Bi = 0.1.

The elevation of suction s enlarges the value of skin friction and Nusselt number, as shown in Figure 4 (a) and 4 (b). These can be clarified by understanding the concept of suction which attracts the flow towards the slab through the small holes, thus intensifies the drag force over the surface. The Nusselt number also enlarges which show that the amplification of s upgrades the rate of heat transmission of the system. The value of critical points depletes as in $\alpha_c = -2.7509$ (s =1.8), $\alpha_c = -2.8688$ (s =1.9) and $\alpha_c = -2.9908$ (s =2.0), which denotes that the detachment of boundary layer is delayed.

(a) (b)

FIGURE 4. (a) $C_f Re_x^{\frac{1}{2}}$ for varied s, (b) $Nu_x Re_x^{-\frac{1}{2}}$ for varied s *and* Δ= 0.1, Rd = 0.5, Ec = 0.01, M = 0.1, G= 0.1, Bi = 0.1.

From Table 3, it is displayed that all parameters radiation Rd, Eckert number Ec, and Biot number Bi do not give any noticeable change to the value of skin friction since they don't really affect the velocity of the liquid. However, the changes are evident for the local Nusselt number since their influences on hybrid nanofluid connect a lot with the temperature. The strengthen of Ec reduces the Nusselt number, which depicts that the rate of heat transmission shrinks. However, the magnification of Rd and Bi boosts the Nusselt number, which depicts that the rate of heat transmission grows. Only magnetic field M does not show any influence on both the skin friction coefficient and local Nusselt number.

TABLE 3. Values of skin friction coefficient and local Nusselt number when $\alpha = -2$ and $\phi_1 = \phi_2 = 0.01$.

Rd	Ec	M	Bi	$C_f Re_x^{\frac{1}{2}}$		$Nu_x Re_x^{-\frac{1}{2}}$	
				1st solution	2nd solution	1st solution	2nd solution
0.5	0.01	0.1	0.1	6.202790552	-0.482517395	0.135690599	0.092410010
1.0	-	-	-	6.202790551	-0.482517394	0.177268218	0.135263474
1.5	-	-	-	6.202790551	-0.482517394	0.217787471	0.169556937
-	0.05	-	-	6.202790570	-0.482517391	0.099712755	-0.054059817
-	0.1	-	-	6.202790577	-0.482517396	0.054740450	-0.237147095
-	-	0.2	-	6.202790552	-0.482517397	0.135512396	0.083085835
-	-	0.3	-	6.202790552	-0.482517397	0.135334194	0.073761663
-	-	-	0.2	6.202790551	-0.482517397	0.262094426	0.162148866
-	-	-	0.3	6.202790551	-0.482517391	0.380133324	0.216647944

As Hartmann number G rises, the rapidity of fluid keeps increasing as demonstrated in Figure 5 (a). The Lorentz force produced helps to accelerate the motion of the flow instead of supressing the movement, which is feasible because the force has a linear connection with the magnetic field and the liquid's velocity. The temperature drops as shown in Fig 5 (b) proves the increment of Nusselt number in Fig 3 (b). This result shows that the amplification of G is not suitable for heat isolation as more heat is absorbed from the fluid instead of into it. Both momentum and thermal boundary layer become thinner as G surges.

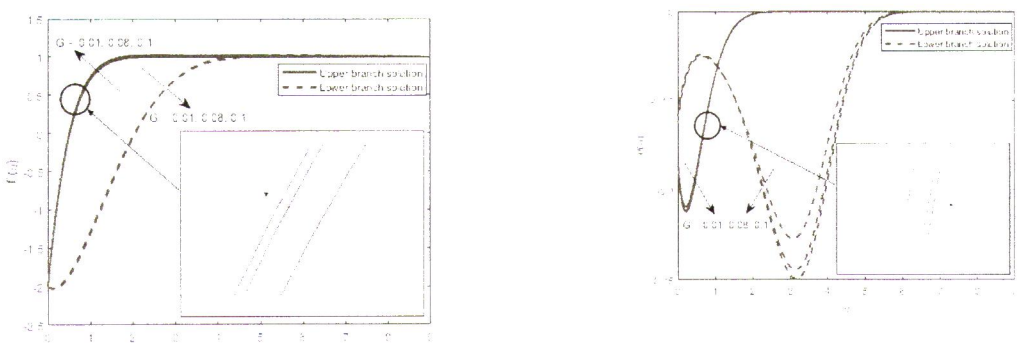

(a) (b)

FIGURE 5. (a) $f'(n)$ for varied G, (b) $\vartheta(n)$ for varied G *and* Δ= 0.1, Rd = 0.5, Ec = 0.01, M = 0.1, s= 2, Bi = 0.1.

Figure 6 (a) illustrates how suction s influences the speed of the flow as it escalates. The movement of the fluid becomes faster, and the thickness of momentum boundary layer depletes. Suction pulls the flow towards the surface, leading to the increment of liquid's motion near that area, hence the augmentation of velocity. The temperature declines as s soars, but then it surges approximately at point $n = 0.43$ as represented in Fig 6 (b). This can be explained by the presence of holes over the plate, that leads to thermal transference out of the fluid at first. However, the temperature begins to rise, and the boundary layers starts to expand at a turning point.

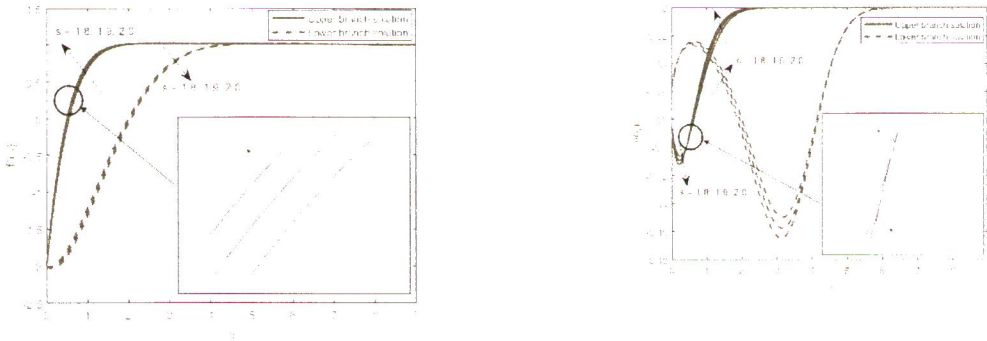

(a) (b)

FIGURE 6. (a) $f'(n)$ for varied s. (b) $\vartheta(n)$ for varied s *and* Δ= 0.1, Rd = 0.5, Ec = 0.01, M = 0.1,G= 0.1, Bi = 0.1.

The effect of magnetic field M towards the temperature is shown is Figure 7. Based on the result, the temperature of the fluid and the thermal boundary layer dwindle as M amplifies. The Lorentz force produced from the field gathers the particles near the moving sheet. Therefore, more heat transference occurs over the plate, less heat is transmitted into the liquid, thus the declination of temperature.

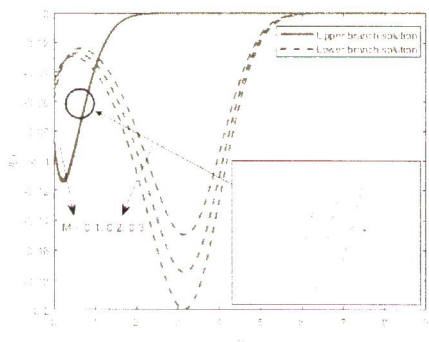

(a)

FIGURE 7. $\vartheta(n)$ for varied M *and* Δ= 0.1, Rd = 0.5, Ec = 0.01, s = 2,G= 0.1, Bi = 0.1.

Figure 8 demonstrates that as radiation Rd magnifies, the temperature shoots up but approximately at n = 0.5, it starts to fall off. At first, due to the heat, the increment of radiation proliferates the clash between the molecules, the generation of kinetic energy grows, and more heat flux is produced. However, the thermal boundary layer begins to lose its thickness at some point which show that the heat is not absorbed into the fluid anymore.

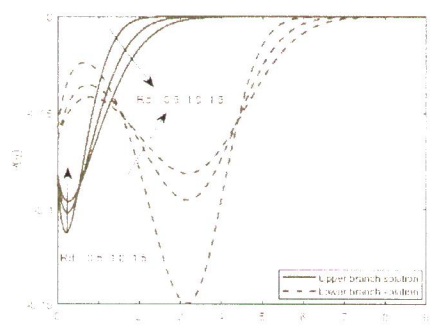

(a)

FIGURE 8. $\vartheta(n)$ for varied Rd *and* Δ= 0.1,M= 0.1, Ec = 0.01, s = 2,G= 0.1, Bi = 0.1.

The influence of Eckert number Ec on the temperature of the fluid is illustrated in Figure 9. It is illustrated that the temperature of the fluid and the thickness of thermal boundary layer deplete as the value of Ec amplified.

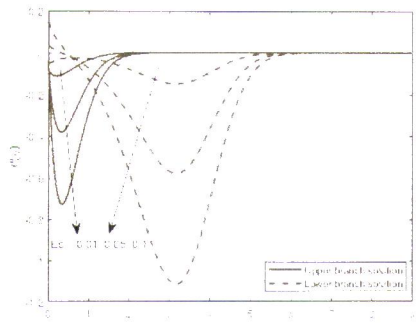

(a)

FIGURE 9. $\vartheta(n)$ for varied Ec *and* Δ= 0.1,M= 0.1, Rd = 0.5, s = 2,G= 0.1, Bi = 0.1.

The influence of Biot number Bi towards the temperature is presented in Figure 10. The temperature lessens as the value of Bi boosts and this is mainly because high amount of Bi tends to actuate the chilling procedures over the plate. This process will decrease the amount of heat transmitted into the particles, hence greatly leads to the decrement of fluid's temperature. Moreover, Bi is directly related to the coefficient of heat transfer and inversely related to the thermal resistance. Hence, as Bi increases, the reduction of thermal resistance will elevate the rate of heat transfer and decrease the temperature.

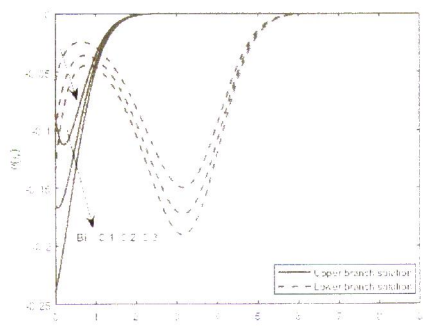

(a)

FIGURE 10. $\vartheta(n)$ for varied Bi *and* Δ= 0.1, M= 0.1, Ec = 0.01, s = 2, G= 0.1, Rd = 0.5.

CONCLUSION

In this paper, the heat transfer characteristics of a hybrid nanofluid GO-MoS_2/H_2O with Joule heating and radiation effects over a pore-filled Riga plate is examined numerically. From the discussions, it can be concluded that:

1. The surface frictional factor is strengthened by Hartmann number and suction.
2. The rate of heat transfer is elevated by higher value of radiation and Biot number.
3. The rapidity of the fluid is boosted by the increment of Hartmann number and suction.
4. Only suction effect will enhance the temperature of fluid.

ACKNOWLEDGMENTS

The authors would like to thank the Ministry of Higher Education Malaysia and the National Defence University of Malaysia for supporting this research, Fundamental Research Grant Scheme, for supporting this research, Fundamental Research Grant Scheme, FRGS/1/2021/STG06/UPNM/02/1.

REFERENCES

1. S. Sangapatanam, K. Subbarayudu and B.R. Polu, J. Therm. Eng., **8(3)**, 445-455 (2022).
2. M. Sheikhpour, M. Arabi, A. Kasaeian, A.R. Rabei and Z. Taherian, Nanotechnol Sci Appl., **13**, 47-59 (2020).
3. M. Bahiraei, R. Rahmani, A. Yaghoobi, E. Khodabandeh, R. Mashayekhi and M. Amani, Appl. Therm. Eng., **133**, 137-159 (2018).
4. N.A.M. Alkuhayli, Mathematics, **11(4)**, 909 (2023).
5. A. Gailitis and O. Lielausus, Appl. Magnetohydrodyn, **12**, 143–146 (1961).
6. J. Kayalvizhi and A. G. V. Kumar, Energies, **15(21)**, 8317 (2022).
7. N. S. Khashi'ie, N. M. Arifin and I. Pop, Mathematics, **8(6)**, 912 (2020).
8. S. Mukhtar and T. Gul, Mathematics, **11(5)**, 1175 (2023).
9. U. Khan, A. Zaib, A. Ishak, I. Waini, J. K. Madhukeshm Z. Raizah and A. M. Galal, Symmetry, **14(7)**, 1312 (2022).
10. R. I. Yahaya, N. M. Arifin, I. Pop, F. M. Ali and S. S. P. M. Isa, Mathematics, **11(1)**, 215 (2023).
11. B. Souayeh, K. Ramesh, N. Hdhiri, E. Yasin, M. W. Alam, K. Alfares and A. Yasin, Nanomaterials, **12(10)**, 1615 (2022).
12. R. Sindhu, N. Alessa, S. Eswaramoorthi and K. Loganathan, Symmetry, **15(1)**, 199 (2023).
13. N. Ahmed, F. Sabam U. Khan, I. Khan, T. A. Alkanhal, I. Faisal and S. T. Mohyud-Din, Energies, **12(1)**, 76 (2019).
14. A. Dawar, S. Islam, A. Alshehri, E. Bonyah and Z. Shah, Journal of Nanomaterials, **2022**, 4903486.
15. S. Ahmad, K. Ali, M. Ashraf, H. A. E. Khalifa, F. A. A. El Seabee and E. M. T. El Din, Nanotechnology Reviews, **11(1)**, 2903-2915 (2022).
16. R. Mansouri, R. Pourrajab, M. Behbahani and A. D. DEzfuli, Journal of Thermal Analysis and Calorimetry volume, **148**, 5765–5776 (2023).
17. A. Hamid, Hashim, A. Hafeez, M. Khan, A. S. Alshomrani and M. Alghamdi, European Journal of Mechanics - B/Fluids, **76**, 434-441 (2019).
18. S. Dinarvand and M. N. Rostami, "Three-dimensional squeezed flow of aqueous magnetite–graphene oxide hybrid nanofluid: A novel hybridity model with analysis of shape factor effects ", in *Journal of Process Mechanical Engineering*, Proceedings of the Institution of Mechanical Engineers, Part E: Journal of Process Mechanical Engineering, (SAGE Publications Inc., 2020), pp. 1-13.
19. G. Huminic, A. Vardaru, A. Huminic, C. Fleaca, F.Dumitrache and I. Morjan, International Journal of Molecular Sciences, **23(6)**, 3056, (2022).
20. B. R. Bharadwaj, K. S. Mogeraya, D. M. Manjunath, B. R. Ponangi, K. S. R. Prasad and V. Krishna, "CFD analysis of heat transfer performance of graphene-based hybrid nanofluid in radiators", in *IOP Conference Series: Materials Science and Engineering*, 346, International Conference on Recent Advances in Materials & Manufacturing Technologies, (IOP Publishing, Dubai, UAE, 2017), 012084.
21. M. Zubair, Z. Shah, A. Dawar, S. Islam, P. Kumam and A. Khan, Entropy, **21(8)**, 747 (2019).
22. H. UR Rasheed, A. Al-Zubaidi, S. Islam, S. Saleem, Z. Khan and W. Khan, Coatings, **11(3)**, 353 (2021).
23. S. Jayanthi and H. Niranjan, Symmetry, **15(2)**, 314 (2023).
24. M. I. Joyce, J. Kandasamy and S. Sivanandam, Mathematical and Computational Applications, **28(1)**, 18 (2023).
25. L. Yan, S. Dero, I. Khan, I. A. Mari, D. Baleanu, K. S. Nisar, E. M. Sherif and H. S. Abdo, Process, **8(3)**, 332 (2020).
26. R. Prabakaran, S. Eswaramoorthi, K. Loganathan and I. E. Sarris, Micromachines, **13(9)**, 1424 (2022).
27. M. K. Narayanaswamy, J. Kandasamy and S. Sivanandam, Mathematical and Computational Applications, **27(6)**, 110 (2022).
28. N. A. Zainal, R. Nazar, K. Naganthran and I. Pop, Mathematics, **10(13)**, 2356 (2022).

29. A. Aziz, Communications in Nonlinear Science and Numerical Simulation, **14(4)**, 1064-1068 (2009).
30. A. Ashraf, Z. Zhang, T. Saeed, H. Zeb and T. Munir, Nanomaterials, **12(7)**, 1152 (2022).
31. N. A. Zainal, R. Nazar, K. Naganthran and I. Pop, Nanomaterials, **12(10)**, 1771 (2022).
32. N. S. Anuar, N. Bachok, N. M. Arifin and H. Rosali, Journal of King Saud University – Science, **33(3)**, 101370, (2021).
33. N. A. Zainal, R. Nazar, K. Naganthran and I. Pop, Mathematics, **8(10)**, 1649 (2020).
34. N. S. Khashi'ie, N. M. Arifin, I. Pop, R. Nazar, E. H. Hafidzuddin and N. Wahim Chinese Journal of Physics, **66**, 157-171 (2020).
35. N. A. Aminuddin, N. A. A. M. Nasir, W. Jamshed, A. Ishak, I. Pop and M. R. Eid, Symmetry, **15(3)**, 584 (2023).
36. N. A. A. M. Nasir, A. Ishak and I. Pop, Journal of Zhejiang University-SCIENCE A (Applied Physics & Engineering), **20(4)**, 290-299 (2019)
37. A. Aziz, W. Jamshed, T. Aziz, H.M.S. Bahaidarah, K.U. Rehman, Journal of Thermal Analysis and Calorimetry, **143**, 1331–1343 (2021).
38. M.A. Qureshi, Case Study of Thermal Engineering, **28**, 101581 (2021).
39. S.P.A. Devi and S. U. Devi, Int. J. Nonlinear Sci. Numerical Simulation, **17**, 249–257 (2016).
40. M. Yaseen, S. K. Rawat, A. Shafiq, M. Kumar and K. Nonlaopon, Symmetry, **14(9)**, 1943 (2022)